THE JOURNAL OF PHYSICAL CHEMISTRY C

Article

pubs.acs.org/JPCC

Surprising Effects of Hydrochloric Acid on the Water Evaporation Coefficient Observed by Raman Thermometry

Anthony M. Rizzuto,[†,‡] Erik S. Cheng,[†] Royce K. Lam,[†,‡] and Richard J. Saykally*[,†,‡]

[†]Department of Chemistry, University of California, Berkeley, California 94720, United States

[‡]Chemical Sciences Division, Lawrence Berkeley National Laboratory, Berkeley, California 94720, United States

Supporting Information

ABSTRACT: The kinetics and energetics of cloud droplet and aerosol formation in the atmosphere are strongly influenced by the evaporation and condensation rates of water, yet the magnitude and mechanism of evaporation remains incompletely characterized. Of particular import (and controversy) is the nature of interfacial water pH and its potential effects on evaporation rate and environmental reactivity. We have used Raman thermometry measurements of freely evaporating microdroplets to determine evaporation coefficients (γ) for two different hydrochloric acid solutions, both of which result in a significant deviation from γ_{water}. At 95% confidence, we find the evaporation coefficient for 1.0 M HCl to be 0.24 ± 0.04, a ∼60% decrease relative to pure water, and for 0.1 M HCl to be 0.91 ± 0.08, a ∼45% *increase* relative to pure water. These results suggest a large perturbation in the surface structure induced by either hydronium ions adsorbing to the water surface or by the presence of a $Cl^-\cdots H_3O^+$ ion-pair moiety in the interfacial region.

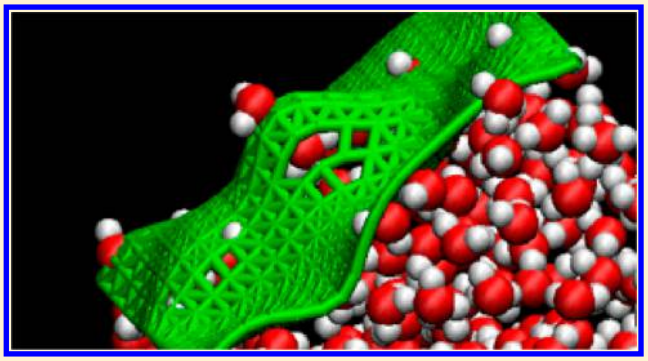

INTRODUCTION

Understanding the detailed mechanism of water evaporation and condensation remains an unsolved fundamental problem. Such processes occurring on the surfaces of micron-sized droplets are vital in atmospheric processes, governing cloud droplet growth kinetics and, in turn, aerosol formation and cloud radiation properties.[1−4] Despite decades of study, the rates of water evaporation and condensation remain controversial, particularly in the case of aerosol droplets containing ions and surfactant molecules.[5−9]

The kinetics of evaporation and condensation processes are governed by the evaporation (γ) and condensation (α) coefficients. Those coefficients are empirically determined ratios of the observed molecular flux evaporating from or condensing onto the liquid surface to the theoretical maximum values permitted by gas kinetic theory. For evaporation, this is described by the Hertz−Knudsen equation:

$$J_e = \gamma \frac{p_{sat}}{\sqrt{2\pi m k_B T_{surf}}} \quad (1)$$

Here, J_e is the evaporative flux, p_{sat} is the saturation vapor pressure of the liquid, T_{surf} is the surface temperature of the liquid, m is the molecular mass of the evaporating molecule, k_B is the Boltzmann constant, and γ is the evaporation coefficient. Because the present work only concerns the study of evaporation rates, we will exclude the condensation coefficient and mass accommodation flux from further discussion except to note that there is an analogous equation for condensation. It is also important to note that microscopic reversibility requires that condensation and evaporation coefficients for a single system be equal, so this study implicitly also reports on the condensation rate.

An evaporation coefficient of unity describes a system with no energetic or entropic barrier to evaporation. An evaporation coefficient of less than unity then describes a system with some kinetic or thermodynamic barrier, such as proceeding through a transition state or a specific orientation that has an associated energetic barrier. As such, determination of an accurate value for γ can give valuable insight into the molecular mechanism of evaporation.

Experimental measurements of γ are challenging, and reported values for pure water span 3 orders of magnitude.[10,11] An extensive review of the measurements made over the past century is provided by Marek and Stroud.[11] It is important to note that different experimental techniques tend to yield drastically different results, and values of γ reported to be less than 0.1 are likely due to surface impurities, as those experiments were performed on stagnant surfaces. Additionally, it is difficult to ensure that evaporation events occur without concomitant recondensation under ambient conditions. Our experimental approach transcends those complications by employing a suitably narrow liquid microjet, modified to form a regular droplet train that is injected into vacuum. This provides a clean, continuously renewed droplet surface and

Received: December 21, 2016
Revised: February 2, 2017
Published: February 6, 2017

DOI: 10.1021/acs.jpcc.6b12851
J. Phys. Chem. C 2017, 121, 4420−4425

ensures condensation-free evaporation. Using this technique, we have previously measured the evaporation coefficient of pure water (both H_2O and D_2O) to be 0.62 ± 0.09 (note that uncertainties are 95% confidence limits for all values quoted herein), a value which indicates a small kinetic or energetic barrier to the evaporation process.[12,13] This technique was also used to study the effect of several inorganic ions on the evaporation rate.[14,15] Duffey et al. recently studied the evaporation rate of aqueous acetic acid solutions in an attempt to investigate the effects of molecular surfactants but observed no significant deviation from that of neat water.[16] In fact, the only aqueous solution exhibiting statistically significant change relative to pure water was 4 M sodium perchlorate, which exhibited $\gamma = 0.47 \pm 0.02$, a ~25% decrease.[14]

In addition to experimental studies of evaporation rates, computational modeling has been performed by many groups. Since evaporation is a very rare event (approximately one water molecule evaporates from a 1 nm^2 patch of a liquid–vapor interface every 10 ns),[17] studies have exploited the microscopic reversibility of the system to determine mass accommodation coefficients. Interestingly, molecular dynamics (MD) simulations determine that there is no kinetic barrier to condensation, and by extension, to evaporation, of pure water such that the value of γ is necessarily unity.[18−21] Varilly and Chandler[17] employed transition path sampling to study water evaporation and concluded that evaporation events become more frequent when the relevant surface site exhibits a predominantly negative mean curvature corresponding to an anomalously large capillary wave event. They also find that the evaporation is well-explained by a simple model of ballistic escape from a deep potential well, with no additional barrier to evaporation beyond the cohesive strength of the liquid. Recently, Nagata et al.[22] used MD simulations at the water–air interface to show that the evaporation of water is enabled by a concerted, ultrafast hydrogen-bond rearrangement of interfacial water. They conclude that the requisite kinetic energy of an evaporated water molecule is provided by well-timed making and breaking of hydrogen bonds involving at least three water molecules at the interface, the recoil of which allows one of the molecules to escape.

The pH of the air–water interface is of fundamental chemical significance and is of particular relevance to atmospheric and environmental sciences. Much recent effort has addressed this fiercely debated topic, but with very conflicting results.[23] Beattie and co-workers conclude that hydroxide, rather than hydronium, is preferentially adsorbed to the interface versus hydronium because of its strong effect on the relative permittivity, as well as having a small region of reduced solvent polarization fluctuations.[24] Mishra et al.[25] used electrospray ionization mass spectrometry (ESI-MS) to study the proton-transfer mechanism of gaseous carboxylic acids, concluding that these proton-transfer reactions confirm the presence of hydroxide ions at the interface, even at very acidic bulk pH levels (pH > 2). Contrarily, classical molecular dynamics simulations by Mucha et al.[26] indicate a stronger propensity for hydronium ions to accumulate at the water surface than hydroxide. These results are supported by ab initio MD simulations from several groups.[27−29] Second harmonic generation spectroscopy studies by Petersen et al.[30] found evidence for an enhanced hydronium concentration at the air–water interface, and a phase-sensitive electronic sum frequency generation experiment performed by Tahara and co-workers determined the interfacial pH of water to be lower than that of the bulk by 1.7.[31] Shen and co-workers[32] used phase-sensitive vibrational sum frequency generation to study the water surface upon the addition of 1.2 M HCl, HI, and NaOH. They find that the surface of the acidic solutions is populated by hydronium ions which affect the interfacial hydrogen bonding structure and reorient the interfacial water molecules, which contributes to forming an icelike surface water structure. The basic solution reveals a small preference for hydroxide adsorption at the interface, but how the ion actually contributes to the interfacial hydrogen bonding structure remains unclear. A recent DFT study conducted by Baer et al.,[33] in fact, concludes that neither H_3O^+ nor OH^- exhibit a significant preference for or aversion to the air–water interface. Interestingly, an earlier computational study by Jagoda-Cwiklik et al.[34] determined that there is no true hydrogen bonding when H_3O^+ acts as an acceptor. Qualitatively, they observe a mild surface affinity and strong surface orientation of hydronium, specifically lending support to the idea that hydronium behaves as a defect in the hydrogen-bonding network of water.

Clearly, establishing the chemical details governing water evaporation rate is of central interest, as is the related question of the pH of the water surface. The present study addresses the effect of bulk HCl (aq) concentration on the evaporation rate of water, and in doing so, provides new insight into the controversial subject of the water surface acidity.

EXPERIMENTAL METHODS

A. Sample Preparation. Hydrochloric acid solutions were prepared volumetrically with 12.1 M HCl stock solution (ACS grade, EMD Millipore) and ultrapure water (18.2 MΩ·cm) from a Millipore system.

B. Apparatus. An experimental apparatus schematic is shown in Figure 1. The droplet train is generated by driving the

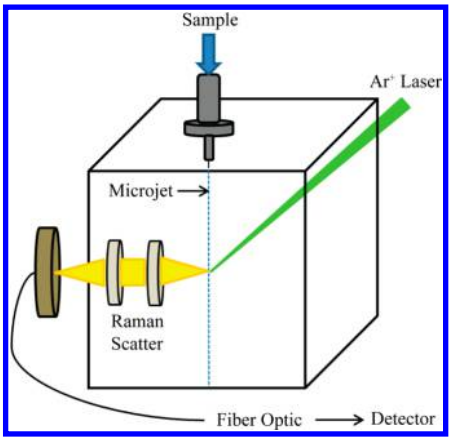

Figure 1. Design of the liquid microjet Raman thermometry experiment.

liquid sample at high pressure (~100 atm) through a 10 ± 1 μm inner diameter fused silica capillary (New Objective). The liquid microjet is mounted on a piezoelectric ceramic which acts as a vibrating orifice aerosol generator (VOAG), and an applied square-wave voltage results in the generation of a uniform periodic droplet train. The microdroplet assembly is mounted on an XYZ-manipulator and attached via bellows to a cubical vacuum chamber with the droplet train propagating downward. The vacuum chamber is evacuated to <100 mTorr by a roughing pump (Varian SD-300). The droplet train is then intersected by an Ar^+ laser beam (Innova 300, Coherent)

DOI: 10.1021/acs.jpcc.6b12851
J. Phys. Chem. C 2017, 121, 4420−4425

operating with ~200 mW at 514.5 nm in the orthogonal direction. The scattered Raman signal is detected at 90° from the incident laser beam and directed to a liquid nitrogen-cooled CCD detector (Princeton Instruments) via an optical fiber. The droplet train is monitored throughout the experiment by measuring the laser light with a photodiode after it passes through the droplet train, which is displayed on an oscilloscope. As each droplet intersects the laser beam there is a dip in signal from the photodiode, resulting in a sinusoidal signal corresponding to the applied square-wave voltage. After the droplets pass through the interaction region, they are frozen onto a liquid nitrogen trap.

C. Raman Thermometry. It has been previously demonstrated that the position and line shape of the −OH stretching vibration in the Raman spectrum of liquid water is highly sensitive to temperature.[35,36] Consequently, one can utilize this feature to measure the temperature of the droplets via a calibrated Raman spectrum. A temperature calibration curve is obtained by collecting the Raman scattering intensity of bulk 0.1 and 1.0 M HCl solutions as a function of temperature over the range 0−30 °C. The calibration temperature is measured using a thermocouple (Sper Scientific) operating at atmospheric pressure. The resulting spectra are baseline corrected and area normalized. The spectra are then divided into two portions: the "low energy stretches" (data below the energy of the isosbestic point) and the "high energy stretches" (data above the energy of the isosbestic point). The two portions of data are individually integrated, and a calibration curve is constructed by plotting the logarithm of the ratios of the integrated portions ($I_{\omega=\text{high}}/I_{\omega=\text{low}}$) against the inverse temperature (K^{-1}). Plots of $\log[I_{\omega=\text{high}}/I_{\omega=\text{low}}]$ vs K^{-1} always exhibit a linear relationship, enabling the straightforward measurement of the temperature of even supercooled water in the droplet train.[37,38]

The residence time of each droplet in vacuum is carefully controlled by adjusting the vertical offset of the microdroplet assembly. By raising the assembly vertically, each droplet resides longer in the vacuum before being probed by the laser. Multiple spectra are recorded at each vertical position of the assembly, assuring reproducibility. Those spectra are then analyzed in the same way as the calibration spectra; they are baseline corrected and area normalized, and then the logarithm of the ratio of the integrated peak areas is determined and compared to the calibration plot. Knowing the vertical distance between the jet aperture and the intersecting laser beam in addition to the liquid flow velocity permits precise calculation of the droplet residence time in vacuum. From these data, as well as the initial droplet size (governed by the orifice inner diameter, the VOAG frequency, and the volumetric flow rate), a cooling curve is generated and compared with the computational model.

D. Cooling Model. The cooling model used has previously been described in detail.[12−16] Briefly, the evaporation rate is described without complications due to condensation, as the droplet radius is generally smaller than the mean free path of evaporating water molecules (~10 μm for these experiments).[12,39] Heat transfer is assumed to occur via conduction only, and the droplet is divided into 20 spherical shells permitting a temperature gradient to form. The surface of the droplet cools as a function of the evaporative flux given by

$$\frac{dT}{dt} = -\gamma \frac{p_{sat}}{\sqrt{2\pi m k_B T}} \frac{\Delta H_{vap}}{C_p} \frac{3r_0^2}{(r_0^3 - r_1^3)\rho} \quad (2)$$

Here, ΔH_{vap} is the enthalpy of vaporization, C_p and ρ are the heat capacity and density of the surface shell, and r is the radius, with the subscripts indicating each subshell (r_0 being the outermost shell). Heat is then conducted outward from each subshell of the droplet:

$$\frac{dQ}{dt} = -\kappa A \frac{dT}{dr} \quad (3)$$

Here Q is heat, κ is the thermal conductivity, and A is the surface area of the subshell. The two equations are numerically integrated, and the physical parameters are adjusted at each time step as a function of temperature.

RESULTS AND DISCUSSION

Cooling curves were obtained for both 1.0 and 0.1 M HCl, with droplet radii ranging from 7 to 10 μm. The evaporation coefficients determined for these experiments are 0.24 ± 0.04 for 1.0 M HCl and 0.91 ± 0.08 for 0.1 M HCl; the reported errors reflect the 95% confidence interval. Figure 2 shows typical experimental cooling curves for 1.0 M HCl (red circles) and 0.1 M HCl (blue diamonds). The overlaid curves correspond to the curves produced using the cooling model and exhibit very good agreement with the experimental data collected for each solution. The middle curve in the figure corresponds to the cooling curve for pure water (γ = 0.62 ± 0.09). Clearly, the cooling curves for both HCl solutions deviate markedly from that of pure water, demonstrating that the presence of HCl significantly perturbs the surface properties of water and, in turn, alters the evaporation rate.

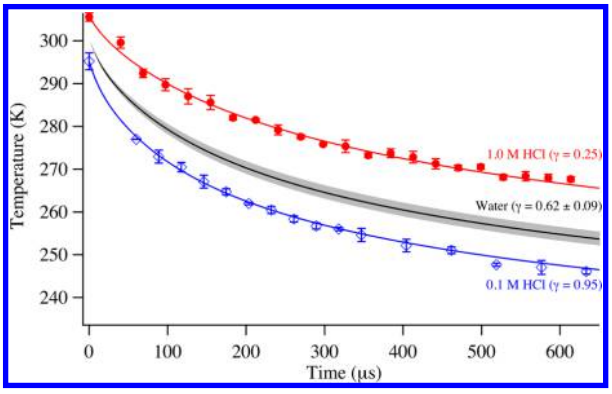

Figure 2. Evaporative cooling curves for 1.0 M HCl (red circles), 0.1 M HCl (blue diamonds), and neat water (black). Cooling curves shown for the HCl solutions are taken from an individual trial. The initial droplet radii were 9.0128 and 7.9859 μm for 1.0 and 0.1 M HCl, respectively. The curves generated from the cooling model are overlaid, showing good agreement between the experiment and the model. The modeled curve for a pure (pH = 7) water droplet initialized with a radius of 9 μm at 300 K is included for reference. The shaded region represents the previously reported uncertainty.

Each experiment has a different initial droplet temperature, depending on the ambient laboratory temperature the day the experiment was performed. To ensure that the apparent difference in γ values for the solutions studied is not an artifact of the variable starting temperature, the cooling model was employed for the three γ values of interest. These data are shown in Figure 3, and it is clear that even with an identical

DOI: 10.1021/acs.jpcc.6b12851
J. Phys. Chem. C 2017, 121, 4420−4425

initial droplet temperature, the generated cooling curves are significantly different for each modeled solution.

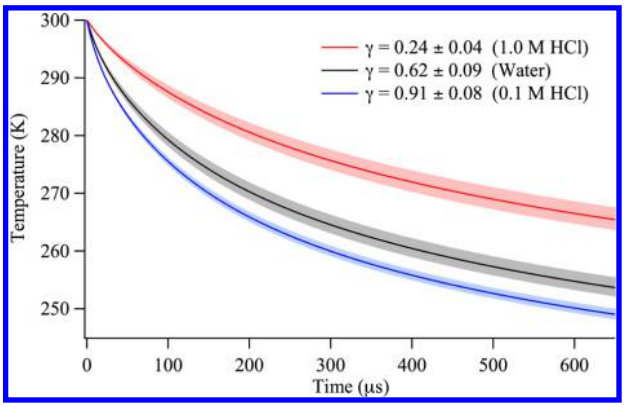

Figure 3. Modeled cooling curves for $\gamma = 0.24$, $\gamma = 0.91$, and $\gamma = 0.62$, corresponding to the measured values for 1.0 M HCl (red), 0.1 M HCl (blue), and pure water (black), respectively. The droplets were initialized with identical temperatures at $t = 0$ s, and with radii of 9 μm at 300 K. Uncertainties for each γ value are depicted by the shaded regions.

Interestingly, the two acid solutions drive the evaporation coefficient in opposite directions. While the 0.1 M HCl solution effects an *increase* in the rate of evaporation ($\gamma_{0.1MHCl}$ is ∼45% greater than γ_{water}), the 1.0 M HCl solution *reduces* that rate by nearly a factor of 3 ($\gamma_{1.0MHCl}$ is ∼60% lower than γ_{water}). These effects can be rationalized if the presence of hydronium significantly perturbs the interfacial hydrogen bond structure of the droplet. Voth and co-workers[40] recently employed quantum simulations to examine the molecular details governing hydronium adsorption to the air−water interface, finding that hydronium is indeed preferentially adsorbed, and that this adsorption results in the pinning of instantaneous surface height fluctuations of water. The pinning was found to affect the surface region encompassed by a ∼6 Å radius around the hydronium ion. The decrease in the entropy from suppressed surface fluctuations agrees with other recent studies of ion adsorption,[41] and the effect on the interfacial hydrogen-bonding network supports our findings here. This suggests that in a 1.0 M HCl solution the hydronium at the surface will pin ∼10% of the interfacial water molecules. This significant amount of interfacial pinning severely dampens the instantaneous surface fluctuations and is the likely source of the marked decrease in the observed evaporation rate, given that Varilly and Chandler have associated evaporation events with capillary waves in their transition path sampling study.[17] By comparison, a 0.1 M HCl solution would only result in pinning ∼1% of interfacial water molecules, a number that is insufficient to dampen the instantaneous surface fluctuations to the point of depressing the evaporation rate. However, those surface-enhanced hydronium ions may be sufficient to reduce the average degree of hydrogen bonding at the interface, making it more thermodynamically favorable for an evaporation event to occur. While this analysis is speculative, it is also consistent with the findings of Nagata et al., which emphasize the importance of detailed ultrafast hydrogen-bond rearrangement dynamics in the evaporation of interfacial water.[22]

Another interesting point concerns the complex issue of ion pairing.[42,43] Some studies have suggested a significant degree of ion pairing between hard acids and soft bases in aqueous solutions.[44−46] Of particular interest is a study by Lewis et al.[46] which found a ∼20% decrease in HNO_3 dissociation at the solution interface compared to bulk. Furthermore, it was determined that the dissociation occurs in the topmost interfacial layer. This implies a significant effect of the interface on the behavior of certain acids. Mundy and co-workers[47] report that the $Cl^-\cdots H_3O^+$ contact ion pair structure also persists through a large concentration range at the air−water interface. An enhanced adsorption of the $Cl^-\cdots H_3O^+$ contact ion pair moiety to the air−water interface would be consistent with the simple thermodynamic adsorption model put forth by Onsager and Samaras,[48] although the adsorption of a mostly un-ionized acid has been shown by Duffey et al. to have little effect on the evaporation rate.[16] While the results of Mundy and co-workers add support to the findings reported here, they did not study HCl solutions at concentrations near 0.1 M, and so we cannot directly compare our results for that concentration. An XAFS study by Fulton et al.[49] also found significant ion pairing for aqueous HCl to the extent that the authors propose a bridged proton structure ($Cl-H-OH_2$) of the ion pair, similar to that of the Zundel ion ($H_2O - H - OH_2^+$). However, the concentrations studied ranged from 6 to 16.1 m, which correspond to HCl/H_2O ratios between 1:9.3 and 1:3.5, and so again we are unable to make direct comparisons to our low concentration experiments. We again note the study by Lewis et al.[46] which actually *does* predict stabilization of the molecular form of the strong acid HNO_3 at the interface even at low concentrations. While this is intriguing, we again are unable to draw a direct comparison as the acids are quite different in terms of size, shape, charge density, etc. If HCl is truly adsorbed to the interface as a contact ion pair moiety, or in the form of a Zundel-like structure, the notion of this acid acting as a defect in the interfacial hydrogen bonding network deserves further study.

■ CONCLUSIONS

We describe the first experimental study of ballistic evaporation performed with the liquid jet Raman thermometry method to identify an aqueous solution exhibiting an evaporation coefficient significantly different from that of pure water. We find that as the concentration of HCl is increased to 0.1 M, the γ value *increases* by ∼45% relative to that of pure water, indicating a decrease in the barrier to free evaporation of water molecules. If the concentration of HCl is increased further, to 1.0 M, the γ value *decreases* by ∼60% relative to that of pure water, indicating a large increase in the barrier to free evaporation of water molecules. These results imply a significant tendency for hydrated protons to adsorb to the droplet surface, either as an isolated ion or in the form of a contact ion pair with its counterion, Cl^-. Further theoretical investigation is clearly needed to clarify the exact mechanism underlying these intriguing effects.

■ ASSOCIATED CONTENT

Supporting Information

The Supporting Information is available free of charge on the ACS Publications website at DOI: 10.1021/acs.jpcc.6b12851.

Cooling model (PDF)

■ AUTHOR INFORMATION

Corresponding Author

*Phone: 510-642-8269. E-mail: saykally@berkeley.edu.

DOI: 10.1021/acs.jpcc.6b12851
J. Phys. Chem. C 2017, 121, 4420−4425

ORCID
Anthony M. Rizzuto: 0000-0002-1430-4414

Notes

The authors declare no competing financial interest.

■ ACKNOWLEDGMENTS

This work was supported by the Director, Office of Basic Energy Sciences, Offices of Science, U.S. Department of Energy (DOE) under Contract No. DE-AC02-05CH11231 through the LBNL Chemical Sciences Division. We thank David Chandler and Patrick Varilly for help in generating the TOC graphic. The data presented are available upon request from saykally@berkeley.edu.

■ REFERENCES

(1) Bones, D. L.; Reid, J. P.; Lienhard, D. M.; Krieger, U. K. Comparing the Mechanism of Water Condensation and Evaporation in Glassy Aerosol. *Proc. Natl. Acad. Sci. U. S. A.* **2012**, *109*, 11613−11618.
(2) Davies, J. F.; Haddrell, A. E.; Miles, R. E. H.; Bull, C. R.; Reid, J. P. Bulk, Surface, and Gas-Phase Limited Water Transport in Aerosol. *J. Phys. Chem. A* **2012**, *116*, 10987−10998.
(3) Ruehl, C. R.; Chuang, P. Y.; Nenes, A. How Quickly Do Cloud Droplets Form on Atmospheric Particles? *Atmos. Chem. Phys.* **2008**, *8*, 1043−1055.
(4) Feingold, G.; Chuang, P. Y. Analysis of the Influence of Film-Forming Compounds on Droplet Growth: Implications for Cloud Microphysical Processes and Climate. *J. Atmos. Sci.* **2002**, *59*, 2006−2018.
(5) Miles, R. E. H.; Davies, J. F.; Reid, J. P. The Influence of the Surface Composition of Mixed Monolayer Films on the Evaporation Coefficient of Water. *Phys. Chem. Chem. Phys.* **2016**, *18*, 19847−19858.
(6) Davies, J. F.; Miles, R. E. H.; Haddrell, A. E.; Reid, J. P. Influence of Organic Films on the Evaporation and Condensation of Water in Aerosol. *Proc. Natl. Acad. Sci. U. S. A.* **2013**, *110*, 8807−8812.
(7) Takahama, S.; Russell, L. M. A Molecular Dynamics Study of Water Mass Accommodation on Condensed Phase Water Coated by Fatty Acid Monolayers. *J. Geophys. Res.* **2011**, *116*, 1−14.
(8) Gilde, A.; Siladke, N.; Lawrence, C. P. Molecular Dynamics Simulations of Water Transport through Butanol Films. *J. Phys. Chem. A* **2009**, *113*, 8586−8590.
(9) Barnes, G. T. The Effects of Monolayers on the Evaporation of Liquids. *Adv. Colloid Interface Sci.* **1986**, *25*, 89−200.
(10) Miles, R. E. H.; Reid, J. P.; Riipinen, I. Comparison of Approaches for Measuring the Mass Accommodation Coefficient for the Condensation of Water and Sensitivities to Uncertainties in Thermophysical Properties. *J. Phys. Chem. A* **2012**, *116*, 10810−10825.
(11) Marek, R.; Straub, J. Analysis of the Evaporation Coefficient and the Condensation Coefficient of Water. *Int. J. Heat Mass Transfer* **2001**, *44*, 39−53.
(12) Smith, J. D.; Cappa, C. D.; Drisdell, W. S.; Cohen, R. C.; Saykally, R. J. Raman Thermometry Measurements of Free Evaporation from Liquid Water Droplets. *J. Am. Chem. Soc.* **2006**, *128*, 12892−12898.
(13) Drisdell, W. S.; Cappa, C. D.; Smith, J. D.; Saykally, R. J.; Cohen, R. C. Determination of the Evaporation Coefficient of D2O. *Atmos. Chem. Phys. Discuss.* **2008**, *8*, 8565−8583.
(14) Drisdell, W. S.; Saykally, R. J.; Cohen, R. C. Effect of Surface Active Ions on the Rate of Water Evaporation. *J. Phys. Chem. C* **2010**, *114*, 11880−11885.
(15) Drisdell, W. S.; Saykally, R. J.; Cohen, R. C. On the Evaporation of Ammonium Sulfate Solution. *Proc. Natl. Acad. Sci. U. S. A.* **2009**, *106*, 18897−18901.
(16) Duffey, K. C.; Shih, O.; Wong, N. L.; Drisdell, W. S.; Saykally, R. J.; Cohen, R. C. Evaporation Kinetics of Aqueous Acetic Acid Droplets: Effects of Soluble Organic Aerosol Components on the Mechanism of Water Evaporation. *Phys. Chem. Chem. Phys.* **2013**, *15*, 11634−11639.
(17) Varilly, P.; Chandler, D. Water Evaporation: A Transition Path Sampling Study. *J. Phys. Chem. B* **2013**, *117*, 1419−1428.
(18) Julin, J.; Shiraiwa, M.; Miles, R. E. H.; Reid, J. P.; Pöschl, U.; Riipinen, I. Mass Accommodation of Water: Bridging the Gap Between Molecular Dynamics Simulations and Kinetic Condensation Models. *J. Phys. Chem. A* **2013**, *117*, 410−420.
(19) Vieceli, J.; Roeselová, M.; Tobias, D. J. Accommodation Coefficients for Water Vapor at the Air/water Interface. *Chem. Phys. Lett.* **2004**, *393*, 249−255.
(20) Tsuruta, T.; Nagayama, G. Molecular Dynamics Studies on the Condensation Coefficient of Water. *J. Phys. Chem. B* **2004**, *108*, 1736−1743.
(21) Morita, A.; Sugiyama, M.; Kameda, H.; Koda, S.; Hanson, D. R. Mass Accommodation Coefficient of Water: Molecular Dynamics Simulation and Revised Analysis of Droplet Train/Flow Reactor Experiment. *J. Phys. Chem. B* **2004**, *108*, 9111−9120.
(22) Nagata, Y.; Usui, K.; Bonn, M. Molecular Mechanism of Water Evaporation. *Phys. Rev. Lett.* **2015**, *115*, No. 236102.
(23) Petersen, P. B.; Saykally, R. J. Is the Liquid Water Surface Basic or Acidic? Macroscopic vs. Molecular-Scale Investigations. *Chem. Phys. Lett.* **2008**, *458*, 255−261.
(24) Gray-Weale, A.; Beattie, J. K. An Explanation for the Charge on Water's Surface. *Phys. Chem. Chem. Phys.* **2009**, *11*, 10994−11005.
(25) Mishra, H.; Enami, S.; Nielsen, R. J.; Stewart, L. A.; Hoffmann, M. R.; Goddard, W. A.; Colussi, A. J. Bronsted Basicity of the Air-Water Interface. *Proc. Natl. Acad. Sci. U. S. A.* **2012**, *109*, 18679−18683.
(26) Mucha, M.; Frigato, T.; Levering, L. M.; Allen, H. C.; Tobias, D. J.; Dang, L. X.; Jungwirth, P. Unified Molecular Picture of the Surfaces of Aqueous Acid, Base, and Salt Solutions. *J. Phys. Chem. B* **2005**, *109*, 7617−7623.
(27) Wick, C. D.; Kuo, I.-F. W.; Mundy, C. J.; Dang, L. X. The Effect of Polarizability for Understanding the Molecular Structure of Aqueous Interfaces. *J. Chem. Theory Comput.* **2007**, *3*, 2002−2010.
(28) Buch, V.; Milet, A.; Vácha, R.; Jungwirth, P.; Devlin, J. P. Water Surface Is Acidic. *Proc. Natl. Acad. Sci. U. S. A.* **2007**, *104*, 7342−7347.
(29) Petersen, M. K.; Iyengar, S. S.; Day, T. J. F.; Voth, G. A. The Hydrated Proton at the Water Liquid/Vapor Interface. *J. Phys. Chem. B* **2004**, *108*, 14804−14806.
(30) Petersen, P. B.; Saykally, R. J. Evidence for an Enhanced Hydronium Concentration at the Liquid Water Surface. *J. Phys. Chem. B* **2005**, *109*, 7976−7980.
(31) Yamaguchi, S.; Kundu, A.; Sen, P.; Tahara, T. Communication: Quantitative Estimate of the Water Surface pH Using Heterodyne-Detected Electronic Sum Frequency Generation. *J. Chem. Phys.* **2012**, *137*, No. 151101.
(32) Tian, C.; Ji, N.; Waychunas, G. A.; Shen, Y. R. Interfacial Structures of Acidic and Basic Aqueous Solutions. *J. Am. Chem. Soc.* **2008**, *130*, 13033−13039.
(33) Baer, M. D.; Kuo, I.-F. W.; Tobias, D. J.; Mundy, C. J. Toward a Unified Picture of the Water Self-Ions at the Air−Water Interface: A Density Functional Theory Perspective. *J. Phys. Chem. B* **2014**, *118*, 8364−8372.
(34) Jagoda-Cwiklik, B.; Cwiklik, L.; Jungwirth, P. Behavior of the Eigen Form of Hydronium at the Air/Water Interface. *J. Phys. Chem. A* **2011**, *115*, 5881−5886.
(35) Walrafen, G. E.; Fisher, M. R.; Hokmabadi, M. S.; Yang, W.-H. Temperature Dependence of the Low- and High-Frequency Raman Scattering from Liquid Water. *J. Chem. Phys.* **1986**, *85*, 6970−6982.
(36) D'Arrigo, G.; Maisano, G.; Mallamace, F.; Migliardo, P.; Wanderlingh, F. Raman Scattering and Structure of Normal and Supercooled Water. *J. Chem. Phys.* **1981**, *75*, 4264−4270.
(37) Suzuki, H.; Matsuzaki, Y.; Muraoka, A.; Tachikawa, M. Raman Spectroscopy of Optically Levitated Supercooled Water Droplet. *J. Chem. Phys.* **2012**, *136*, No. 234508.
(38) Smith, J. D.; Cappa, C. D.; Wilson, K. R.; Cohen, R. C.; Geissler, P. L.; Saykally, R. J. Unified Description of Temperature-Dependent

DOI: 10.1021/acs.jpcc.6b12851
J. Phys. Chem. C 2017, 121, 4420−4425

Hydrogen-Bond Rearrangements in Liquid Water. *Proc. Natl. Acad. Sci. U. S. A.* **2005**, *102*, 14171−14174.
(39) Faubel, M.; Kisters, T. Non-Equilibrium Molecular Evaporation of Carboxylic Acid Dimers. *Nature* **1989**, *339*, 527−529.
(40) Tse, Y.-L. S.; Chen, C.; Lindberg, G. E.; Kumar, R.; Voth, G. A. Propensity of Hydrated Excess Protons and Hydroxide Anions for the Air−Water Interface. *J. Am. Chem. Soc.* **2015**, *137*, 12610−12616.
(41) Otten, D. E.; Shaffer, P. R.; Geissler, P. L.; Saykally, R. J. Elucidating the Mechanism of Selective Ion Adsorption to the Liquid Water Surface. *Proc. Natl. Acad. Sci. U. S. A.* **2012**, *109*, 701.
(42) Collins, K. D. Charge Density-Dependent Strength of Hydration and Biological Structure. *Biophys. J.* **1997**, *72*, 65−76.
(43) Collins, K. D.; Washabaugh, M. W. The Hofmeister Effect and the Behaviour of Water at Interfaces. *Q. Rev. Biophys.* **1985**, *18*, 323−422.
(44) Baer, M. D.; Tobias, D. J.; Mundy, C. J. Investigation of Interfacial and Bulk Dissociation of HBr, HCl, and HNO_3 Using Density Functional Theory-Based Molecular Dynamics Simulations. *J. Phys. Chem. C* **2014**, *118*, 29412−29420.
(45) Sun, Z.; Zhang, W.; Ji, M.; Hartsock, R.; Gaffney, K. J. Contact Ion Pair Formation between Hard Acids and Soft Bases in Aqueous Solutions Observed with 2DIR Spectroscopy. *J. Phys. Chem. B* **2013**, *117*, 15306−15312.
(46) Lewis, T.; Winter, B.; Stern, A. C.; Baer, M. D.; Mundy, C. J.; Tobias, D. J.; Hemminger, J. C. Does Nitric Acid Dissociate at the Aqueous Solution Surface? *J. Phys. Chem. C* **2011**, *115*, 21183−21190.
(47) Baer, M. D.; Fulton, J. L.; Balasubramanian, M.; Schenter, G. K.; Mundy, C. J. Persistent Ion Pairing in Aqueous Hydrochloric Acid. *J. Phys. Chem. B* **2014**, *118*, 7211−7220.
(48) Onsager, L.; Samaras, N. N. T. The Surface Tension of Debye-Hückel Electrolytes. *J. Chem. Phys.* **1934**, *2*, 528−536.
(49) Fulton, J. L.; Balasubramanian, M. Structure of Hydronium (H_3O^+)/Chloride (Cl^-) Contact Ion Pairs in Aqueous Hydrochloric Acid Solution: A Zundel-like Local Configuration. *J. Am. Chem. Soc.* **2010**, *132*, 12597−12604.

DOI: 10.1021/acs.jpcc.6b12851
J. Phys. Chem. C 2017, 121, 4420−4425